Available online at www.sciencedirect.com
SCIENCE DIRECT®
Remote Sensing of Environment 89 (2004) 200–216
Remote Sensing of Environment
www.elsevier.com/locate/rse

Evaluating image-based estimates of leaf area index in boreal conifer stands over a range of scales using high-resolution CASI imagery

Richard A. Fernandes[a,*], John R. Miller[b,1], Jing M. Chen[c,2], Irene G. Rubinstein[d,3]

[a] Environmental Monitoring Section, Canada Centre for Remote Sensing, 588 Booth Street, 4th Floor, Ottawa, Ontario, Canada K1A 0Y7
[b] Department of Physics and Astronomy, York University, Petrie Science Building, Room 255, 4700 Keele Street, Toronto, Ontario, Canada M3J 1P3
[c] Department of Geography, 5th Floor Sydney Smith Hall, University of Toronto, 100 ST. George Street, Toronto, Ontario, Canada M5G 3S3
[d] Centre for Research in Earth and Space Technology, Computer Methods Building, 4850 Keele Street, Toronto, Ontario, Canada M3J 1P3

Received 16 February 2001; received in revised form 18 June 2001; accepted 15 June 2002

Abstract

Leaf area index (LAI) is an important surface biophysical parameter as a measure of vegetation cover, vegetation productivity, and as an input to ecosystem process models. Recently, a number of coarse-scale (1-km) LAI maps have been generated over large regions including the Canadian boreal forest. This study focuses on the production of fine-scale (≤ 30-m) LAI maps using the forest light interaction model-clustering (FLIM-CLUS) algorithm over selected boreal conifer stands and the subsequent comparison of the fine-scale maps to coarse-scale LAI maps synthesized from Landsat TM imagery. The fine-scale estimates are validated using surface LAI measurements to give relative root mean square errors of under 7% for jack pine sites and under 14% for black spruce sites. In contrast, finer scale site mean LAI ranges between 49% and 86% of the mean of surface estimates covering only part of the sites and 54% to 110% of coarse-scale site mean LAI. Correlations between fine-scale and coarse-scale estimates range from near 0.5 for 30-m coarse-scale images to under 0.3 to 1-km coarse-scale images but increase to near 0.90 after imposing fine-scale zero LAI areas in coarse-scale estimates. The increase suggests that coarse-scale image-based LAI estimates require consideration of sub-pixel open areas. Both FLIM-CLUS and coarse-scale site mean LAI are substantially lower than surface estimates over northern sites. The assumption of spatially random residuals in regression-based estimates of LAI may not be valid and may therefore add to local bias errors in estimating LAI remotely. Differences between fine-scale airborne LAI maps and 30-m-scale Landsat TM LAI maps suggests that, for sparse boreal conifer stands, LAI maps produced from Landsat TM alone may not always be sufficient for validation of coarser scale LAI maps. In addition, previous studies may have used biased LAI estimates over the study site. Fine-scale spatial LAI maps offer one means of assessing and correcting for effects of sub-pixel open area patches and for characterising the spatial pattern of residuals in coarse-scale LAI estimates in comparison to the true distribution of LAI on the surface.

Keywords: Leaf area index; Validation; Scaling; CASI; Landsat TM; LAI-2000; Effective leaf area index; BOREAS; Boreal conifers; FLIM-CLUS; Reflectance models

1. Introduction

Leaf area index (LAI, alternatively denoted as L), defined as half the total surface area of green foliage per unit of ground area projected on the local horizontal datum, is an important parameter in models of carbon and vapour fluxes between the atmosphere and land surfaces. LAI estimates have been derived over boreal forests from satellite imagery at scales ranging from 30 m (e.g., Chen & Cihlar, 1996; Nilson, Anniste, Lang, & Praks, 1999) to over 1 km (e.g., Chen & Cihlar, 1999; Knyazikhin et al., 2000; Myneni, Nemani, & Running, 1997). These estimates are used for scaling leaf level measurements to stands (Dang et al., 1997), estimating model input parameters (Schaudt & Dickinson, 2000), and as direct input to ecosystem process models (Frolking et al., 1996; Nijssen, Haddeland, & Lattenmaier, 1996; Kimball, Thornton, White, & Running, 1997; Kimball, White, & Running, 1997; Liu, Chen, Cihlar,

* Corresponding author. Fax: +1-613-947-1206.
E-mail addresses: rfernand@ccrs.nrcan.gc.ca (R.A. Fernandes), jrmiller@terra.phys.yorku.ca (J.R. Miller), chenj@geog.utoronto.ca (J.M. Chen), rubin@eol.crestech.ca (I.G. Rubinstein).
[1] Tel.: +1-417-728-2400.
[2] Tel.: +1-416-946-3886.
[3] Tel.: +1-416-665-3311.

0034-4257/$ - see front matter © 2003 Elsevier Inc. All rights reserved.
doi:10.1016/j.rse.2002.06.005

& Chen, 1999). Bonan (1993) and Kimball, Running, and Saatchi (1999) demonstrate that flux estimates from simulation models are sensitive to the spatial scale of input LAI. For example, Kimball et al. (1999) estimate that LAI at 30-m scale explains between 47% and 62% of variance in annual NPP and between 79% and 85% variance in annual ET within a boreal region. Validation of LAI is therefore a priority both for application that use LAI as a direct bio-indicator and as an input to diagnostic or predictive models (Justice, Starr, Wickland, Privette, & Suttles, 1998).

In this paper, both LAI and effective leaf area index (LAI_e, alternatively denoted as L_e) are used. LAI_e is not a physical quantity. Rather, it is related to canopy gap fraction (Nilson, 1971). LAI_e is typically estimated from measurements of the canopy gap fraction at zenith angle θ, $P(\theta)$, assuming a modified Beer–Lambert formulation (Chen & Black, 1992):

$$L_e = \frac{-\ln P(\theta)\cos\theta}{G(\theta)} \quad (1)$$

Where G is the fraction of foliage projected on a plane normal to θ. In this study, the LAI-2000 Plant Canopy Analyser (Welles & Norman, 1991) was used to estimate LAI_e using a discrete approximation to Miller's (1967) theorem:

$$L_e = 2\int_0^{\frac{\pi}{2}} -\ln[P(\theta)]\cos\theta\sin\theta \mathrm{d}\theta \quad (2)$$

The LAI-2000 estimates of LAI_e are typically biased due to multiple scattering, insufficient angular sampling, and clumping (Leblanc & Chen, 2001; Nilson, 1999). LAI can be estimated using LAI_e with additional consideration for the variation in structural parameters with zenith angle, θ, and correction for local surface slope, β:

$$L = \frac{\gamma_E(\theta)[1-\alpha(\theta)]L_e}{\Omega_E(\theta)\cos\beta} \quad (3)$$

The woody-to-total area ratio, α, is typically calibrated by destructive sampling at each site. The needle-to-shoot area ratio, γ_E, can be estimated by analysis of shoots provided in Chen, Rich, Gower, Norman, and Plummer (1997). The clumping factor, Ω_E, describes the deviation of foliage from a random spatial distribution at scales coarser than the shoot. It can be estimated using the Tracing Radiation in Canopies (TRAC) instrument (Chen, 1996a). Estimation of α, γ_E, and Ω_E is the major source of error in surface LAI estimates based on LAI-2000 estimates of LAI_e (Fernandes et al., 2001). Since the emphasis of our study was to assess scaling errors, we also assumed constant values for α, γ_E, and Ω_E across each study site that were applied to all algorithms at all spatial scales. Therefore, all LAI estimates reported in this study have the same bias since they are all calibrated with LAI-2000 measurements.

A number of studies demonstrate the use of surface LAI estimates to calibrate remotely sensed measurements but do not test the estimates with independent validation data sets (Brown, Chen, Leblanc, & Cihlar, 2000; Chen & Cihlar, 1996; Chen et al., 1999; Lefsky et al., 1999; Myneni et al., 1997; Nemani, Pierce, Running, & Band, 1993; Nilson et al., 1999; Peddle, Hall, & LeDrew, 1999; Peterson, Spanner, Running, & Teuber, 1987; Turner, Cohen, Kennedy, Fassnacht, & Briggs, 1999). The coefficient of determination or sample estimate of the Pearson correlation coefficient and, in some cases, the standard error (S.E.) or root mean square error (rmse) is provided. However, measurement errors in both LAI and vegetation indices may often be of similar magnitude (Fernandes et al., 2001) so a Type II (structural) regression (Kendall & Stuart, 1951) is more appropriate than the Type I regression models used in the studies cited above. Nilson et al. (1999) report a relative S.E. for LAI_e between 30% and 40% over 15 boreal conifer stands in Scandinavia. Peddle et al. (1999) demonstrate that shadow fraction from a reflectance model predicts LAI with an S.E. of 0.55 (relative S.E. 22%) over 31 boreal black spruce stands in Minnesota, USA. Lucas, Curran, Plummer, and Danson (2000) use independent validation stands to arrive at a rmse of 0.9 for LAI (relative rmse 10%) using a predictive relationship calibrated with a red edge index. Bicheron and Leroy (1999) report an rmse of 0.95 for LAI (relative rmse 41%) over 14 independent validation stands over the BOREAS region based of inversion of multiangle airborne polarisation and directionality of the Earth's reflectance (POLDER) data via a physically based reflectance model.

All of the reviewed studies use homogenous stands and produce a single LAI estimate per stand. The use of relatively homogenous stands may increase the precision of plot-based LAI estimates in comparison to image-based LAI estimates that adopt an arbitrary sampling grid (Wulder, 1998). One solution to this limitation is to acquire an extensive and representative spatial sampling of LAI within a region (Cohen & Justice, 1999). A complimentary approach is to compare different image-based LAI estimates over the same region. Estimates of the accuracy and precision of LAI estimates of each image product are required for the image-based approach to be meaningful.

In our paper, we use surface LAI estimates to validate LAI maps of selected stands produced using high spatial-resolution compact airborne spectrographic imager (CASI) images. Importantly, the CASI LAI maps are independent of the surface LAI data as they are derived from a canopy reflectance model (forest light interaction model-clustering, FLIM-CLUS; Fernandes, Hu, MIller, & Rubinstein, 2002). The validated CASI LAI maps are then compared to LAI estimates from Landsat TM 5 imagery synthetically smoothed to scales as coarse as 1 km. As a result, our method offers an explicit comparison of both the spatial pattern of LAI and site mean LAI over the study sites. It is noteworthy that the FLIM-CLUS based fine-scale LAI estimates are produced using site-specific information re-

Table 1
Description of study sites including average stand parameters

Stand	Latitude °N	Longitude °W	Dominant overstory	Age (years)	Basal area (m^3 ha^{-1})	Tree height (m)
NSA-OBS	55.880	98.484	*Picea mariana*	75	12	8
NSA-OJP	55.928	98.624	*Pinus banksiana*	58	9.1	12
SSA-OBS	53.987	105.122	*Picea mariana*	155	30	10
SSA-OJP	53.916	104.692	*Pinus banksiana*	75	33	15

NSA corresponds to BOREAS Northern Study Area, SSA corresponds to Southern Study Area, OBS corresponds to Old Black Spruce and OJP corresponds to Old Jack Pine.

garding typical crown-architecture and endmember reflectance. However, our approach supports the role of the fine-scale imagery as a means of spatial validation of coarser resolution LAI maps.

2. Objectives

The objectives of our study are to compare

1. LAI estimates derived using measurements from spatially coincident surface and airborne sensors;
2. site mean LAI estimates based on airborne and satellite sensors;
3. spatial patterns of LAI estimates from airborne sensors derived at ≤ 30 m scale and satellite-based sensors derived at scales ranging from 30 m to 1 km.

In this paper, we define spatial scale as the representative linear dimension of a region of support for a measurement or estimate (e.g., the projected instantaneous field of view or PIFOV of a remote sensing instrument). We use the term grid resolution for the linear dimensions of the region over which measurements or estimates are represented (e.g., the grid size of raster data layers).

3. Study sites and data

Our study was located within the Boreal Ecosystem Atmosphere Study (BOREAS) region in central Saskatchewan and northern Manitoba, Canada (Halliwell and Apps, 1997; Sellers et al., 1993) and consisted of four mature conifer sites where surface, airborne, and satellite measurements were conducted with sufficient precision and ancillary data to allow reliable LAI estimates. A mature black spruce (*Picea mariana* [Mill.] BSP site) (Old Black Spruce or OBS) site and a mature jack pine (*Pinus banksiana* [Lamb.]) (Old Jack Pine or OJP) site were selected within each of two study areas located at the northern (labelled NSA) and southern (labelled SSA) extents of the central Canadian boreal ecosystem (Table 1). In general, all of the sites were larger than 1 km in each horizontal dimension and exhibited relief at horizontal scales coarser than 25 m of less than 1 m. Surface LAI estimates for the selected sites have been used for validation of ecosystem process models using tower flux measurements (Frolking et al., 1996; Nijssen et al., 1996; Kimball, Thornton, et al., 1997; Kimball, White, et al., 1997) and scaling leaf level measurements to stand level (Dang et al., 1997; Gower et al., 1997; Liu et al., 1999). Furthermore, these sites are also part of the MODIS Land Validation Plan (Morisette, Privette, Justice, & Running, 1999).

Compact airborne spectrographic imager (CASI) imagery was acquired during winter 1994, with a nominal 2-m PIFOV over each tower flux site. The canopy was virtually snow-free during image acquisition. Surface LAI estimates were provided for the growing season and during senescence in 1994 (Chen et al., 1997) along 300-m transects in each of the four study sites. Landsat TM 5 at sensor radiance imagery was acquired during the 1994 growing season (Table 2).

LAI measurements from 46 auxiliary sites (Chen et al., 1997) outside the four selected study sites but within the

Table 2
Description of study site data

Site	Surface LAI dates		CASI date[a]	TM 5 date[a]	Surface L[b]	FLIM-CLUS L[c]	RSR 30 m L[d]	RSR 1 km L[d]	Registration error (m)
	Summer	Fall							
NSA-OBS	June 10	September 2	February 10	June 6 (37/22)	3.64	2.04	1.97	1.91	7.5
NSA-OJP	June 11	September 7	February 10	June 6 (37/22)	1.63	1.37	1.37	1.24	11.0
SSA-OBS	June 4	September 11	February 8	June 9 (34/21)	3.67	1.94	3.71	3.62	7.5
SSA-OJP	May 26	September 10	February 7	June 9 (34/21)	2.17	1.86	2.81	2.37	11.0

[a] All dates are for 1994. LANDSAT TM 5 dates are followed by WRS-2 path and row.
[b] Mean summer L over surface transects except for NSA-OBS where three additional samples are included.
[c] Mean summer L over extent of CASI scene at ≤ 30-m scale and 2-m resolution using FLIM-CLUS.
[d] Mean summer L over extent of CASI scene using the Reduced Simple Ratio with LANDSAT TM 5 data.

BOREAS region were used to generate empirical relations for estimating satellite-based LAI that were then applied over the study sites. The sites represent calibration data used for coarse-scale empirical LAI estimates in Chen (1996b), Chen and Cihlar (1996), Chen (1999), and Brown et al. (2000). The auxiliary sites are described in Halliwell and Apps (1997).

4. Methods

Our approach to meeting the objectives involved three types of LAI estimates: surface estimates ("surface"), fine-scale image-based estimates ("fine scale"), and coarser scale image-based estimates ("coarse scale"). Surface estimates were based on measurements along a few transects in each site (except for three additional point samples at the NSA-OBS) and were therefore not used in comparison of spatial patterns over entire sites. The other estimates covered each site at a fixed grid resolution (2 m for fine scale and 30 m for coarse scale) but over a range of spatial scales (2 m for fine scale and between 500 m and 1 km for coarse scale).

4.1. Surface method

The surface estimates (Table 2) were used to validate and calibrate the fine- and coarse-scale estimates. We used the LAI-2000 to estimate LAI_e and multiplied this estimate by 1.15 to correct for multiple scattering (Chen et al., 1997). Parameters required in Eq. (1) to convert from LAI_e to LAI were taken from Chen et al. (1997).

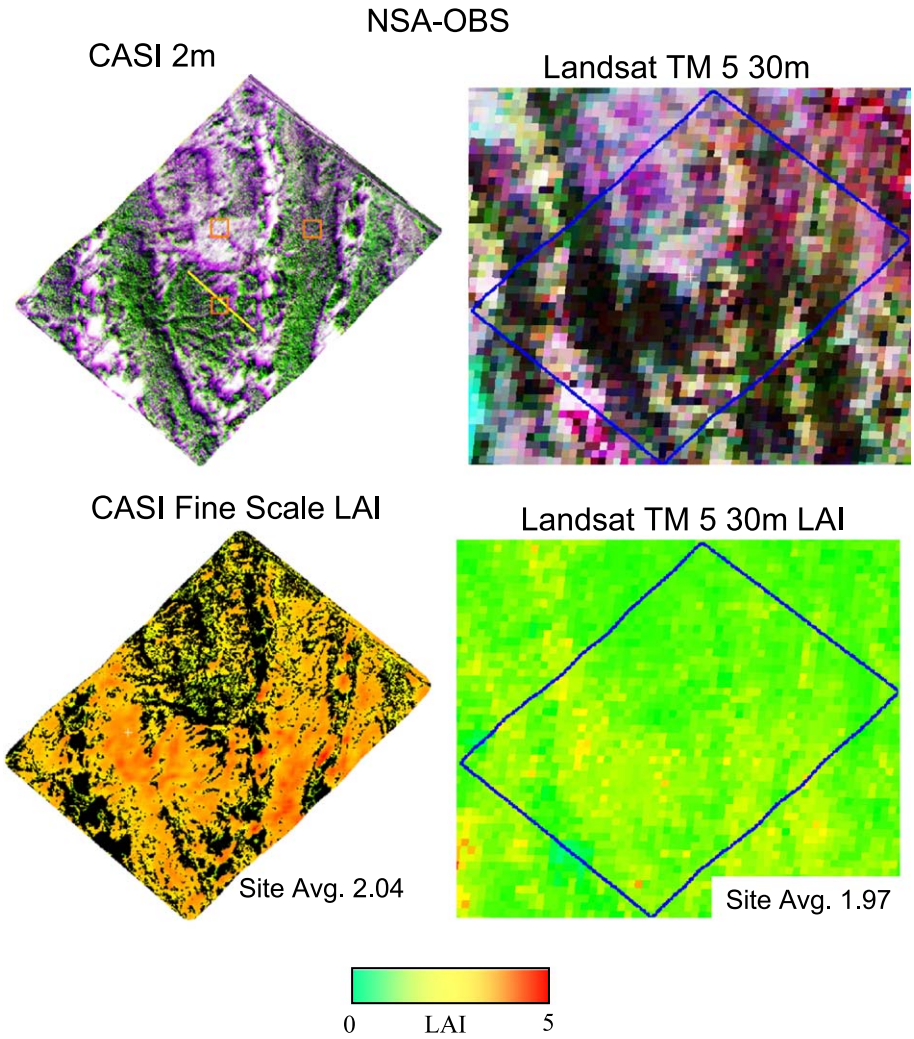

Fig. 1. Imagery and sample LAI maps for the NSA-OBS site. CASI 2-m-resolution red, blue, NIR colour composite image from February 10, 1994 (yellow bar represents 300-m surface LAI-2000 LAI transect, and orange squares represent the spatial footprint of additional TRAC LAI measurements). Landsat TM 5 30-m-resolution red, NIR, SWIR colour composite from June 6, 1994 (blue outline corresponds to CASI image extents). FLIM-CLUS LAI estimate using 2-m-resolution CASI imagery. Landsat TM 5 LAI estimate using the reduced simple ratio at 30-m scale. Imagery has been histogram equalized. A single colour scale is used to represent LAI estimates corrected to early summer levels.

The one standard deviation intervals of measurement errors in surface LAI is approximately 20% for conifer stands and 15% for broadleaf stands (Fernandes et al., 2001) using the measurement methods in Chen (1996b). An additional source of error was seasonal variability in LAI since the image-based estimates were generated in winter for fine-scale and early summer for coarse-scale estimates. We used surface estimates within 1 week of the coarse-scale image data. Post-senescence fine-scale LAI_e estimates were required to adjust the winter fine-scale estimates to equivalent early summer values. Chen and Cihlar (1996) suggest LAI_e for these sites changed less than 5% seasonally, so we assume this correction will be at least as precise.

The field of view of the LAI-2000 estimate spans a circle of radius approximately 3.5 times the canopy height (Welles & Norman, 1991). Surface LAI_e estimates for the auxiliary sites were acquired along two perpendicular 50-m transects crossing the center of each stand. The study sites had three parallel transects between 200 and 300 m long. Additional LAI measurements at three point locations in the NSA-OBS (Dr. Peter White, personal communication) are included in the analysis.

4.2. Fine-scale method

The FLIM-CLUS algorithm (Fernandes et al., 2002) was used to produce 2-m grid resolution estimates of L_e over

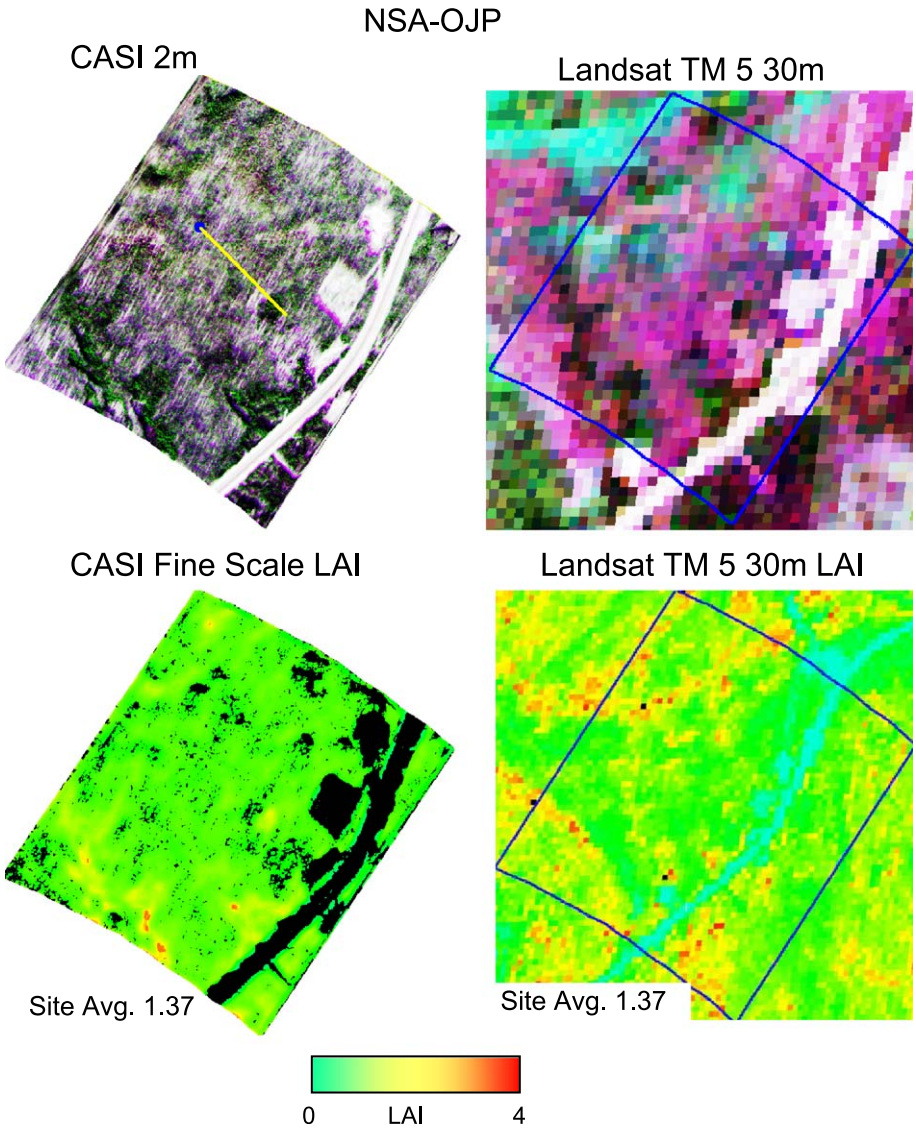

Fig. 2. Imagery and sample LAI maps for the NSA-OJP site. CASI 2-m-resolution red, blue, NIR colour composite image from February 10, 1994 (yellow bar represents 300-m surface LAI-2000 LAI transect). Landsat TM 5 30-m-resolution red, NIR, SWIR colour composite from June 6, 1994 (blue outline indicates the extents of the CASI imagery). FLIM-CLUS LAI estimate using 2-m-resolution CASI imagery. Landsat TM LAI estimate using the reduced simple ratio at 30-m scale. Imagery has been histogram equalized. A single colour scale is used to represent LAI estimates corrected to early summer levels.

each tower site. This section gives an overview of the algorithm. Details regarding the implementation of FLIM-CLUS and its application to the OBS stands are given in Fernandes et al. (2002).

FLIM-CLUS is designed for application to high-resolution winter images of conifer stands as it relies on the spectral and brightness contrast between snow and vegetation to identify open areas. Blue (449–521 nm), red (650–682 nm) and near-infrared (776–821 nm, NIR) CASI radiances were corrected to apparent reflectance using CAM5S (O'Neill et al., 1997) and in situ measurements of aerosol optical depth at 550 nm. The blue band is used since snow has a higher blue reflectance than does a vegetation canopy and shadows and because of low blue reflectance variability over snow (Wiscombe & Warren, 1980). A blue band also improves estimation of forest cover when used in conjunction with red and infrared bands (Horler & Ahern, 1986). Furthermore, reflectance estimates in the blue region based on airborne radiance observations are subject to lower noise due to atmospheric scattering in comparison to satellite-based measurements. The red and NIR channels were included for two reasons. Firstly, vegetation can be distinguished from the snow background using these wavelengths (Hu, Iannen, & Miller, 2000). Secondly, there are a number of studies documenting the relationship between conifer LAI (or effective LAI depending on measurement technique) and information contained in the combination of red and NIR bands (Chen and Cihlar, 1996; Peterson et al., 1987; Rosema, Verhoef, Noorbergen, & Borgesius, 1992; Running, Peterson, Spanner, & Teuber, 1986; Spanner et al., 1994). A shortwave infrared band (e.g., 1.5–1.75 μm) was not available on the CASI sensor,

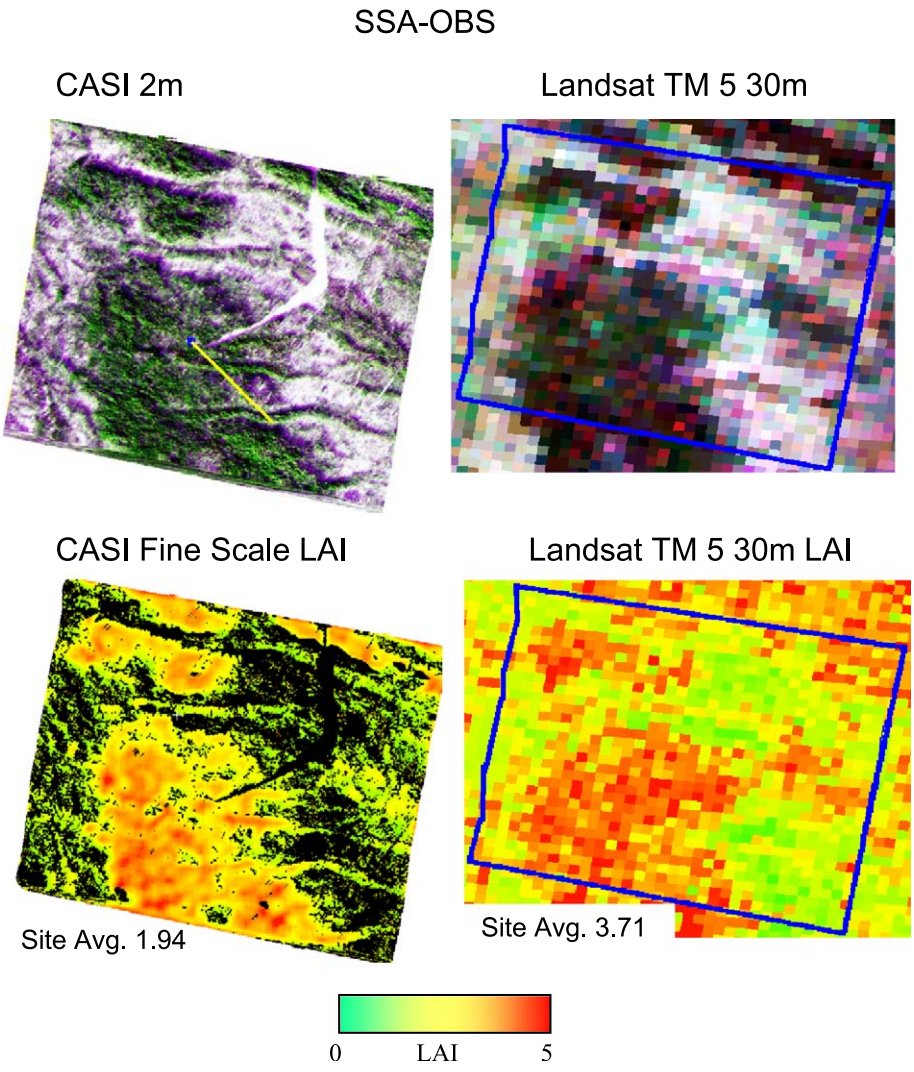

Fig. 3. Imagery and sample LAI maps for the SSA-OBS site. CASI 2-m-resolution red, blue, NIR colour composite image from February 8, 1994 (yellow bar represents 300-m surface LAI-2000 LAI transect). Landsat TM 5 30-m-resolution red, NIR, SWIR colour composite from June 9, 1994 (blue outline corresponds to CASI image extents). FLIM-CLUS LAI estimate using 2-m-resolution CASI imagery. Landsat TM LAI estimate using the reduced simple ratio at 30-m scale. Imagery has been histogram equalized. A single colour scale is used to represent LAI estimates corrected to early summer levels.

so the potential information related to LAI in this wavelength region (e.g., Nemani et al., 1993) could not be applied.

The images are georeferenced (Gray et al., 1997) followed by a linear shift introduced manually in post-processing to bring the visually observed tower position to the known tower coordinates. The manual georeferencing compensates for the consequences of single on-board GPS selective-availability errors. Tests over BOREAS sites indicate a maximum absolute error below 10 m and relative error near 2 m (Dr. Pablo Zarco-Tejeda, personal communication). The georeferenced images together with fine-scale LAI are shown in Figs. 1–4.

The FLIM-CLUS approach begins by identifying regions that can be considered to be part of a vegetation canopy (canopy areas) where a vegetation reflectance model is

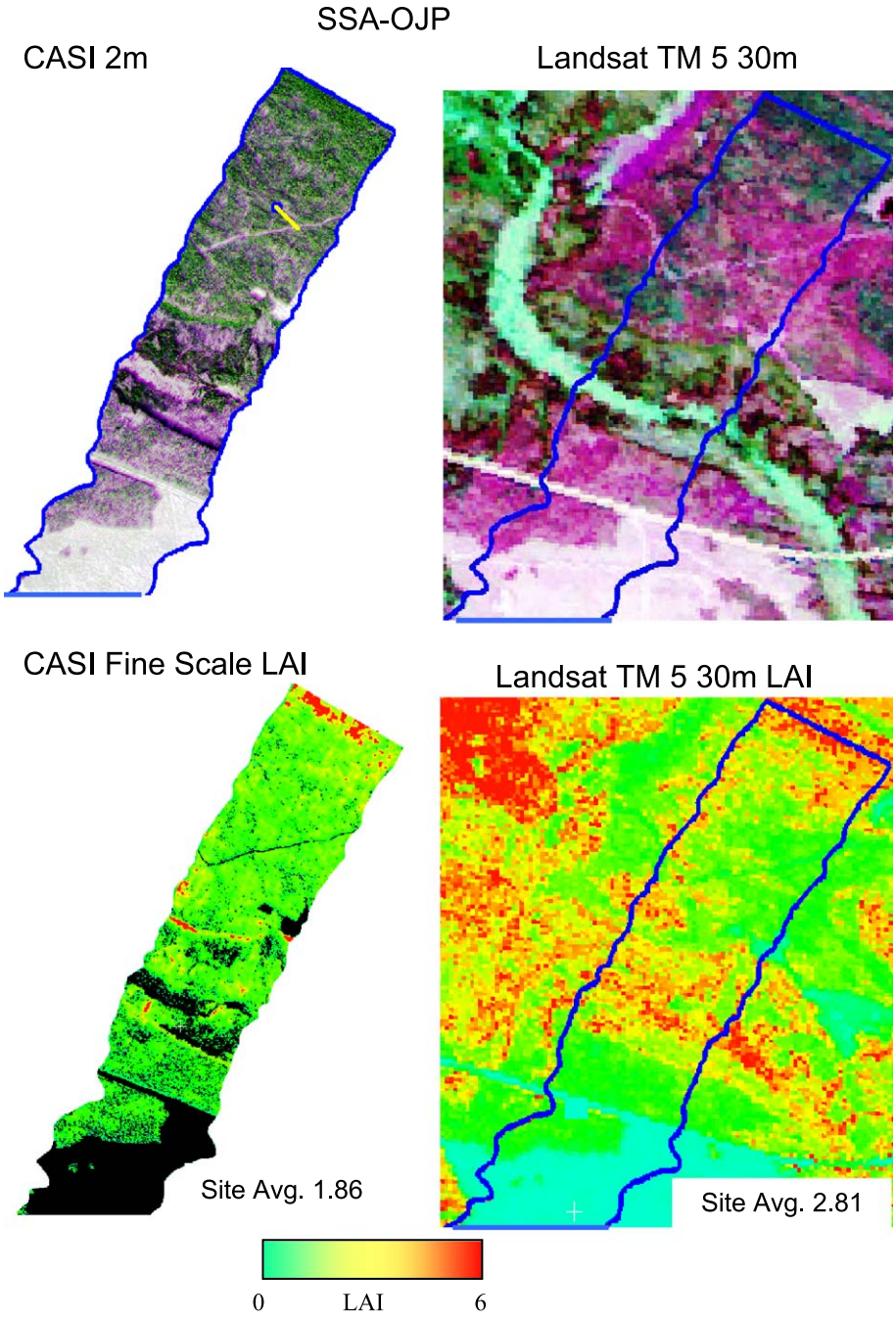

Fig. 4. Imagery and sample LAI maps for the SSA-OJP site. CASI 2-m-resolution red, blue, NIR colour composite image from February 7, 1994 (yellow bar represents 300-m surface LAI-2000 LAI transect). Landsat TM 5 30-m-resolution red, NIR, SWIR colour composite from June 9, 1994 (blue outline corresponds to CASI image extents). FLIM-CLUS LAI estimate using 2-m-resolution CASI imagery. Landsat TM LAI estimate using the reduced simple ratio at 30-m scale. Imagery has been histogram equalized. A single colour scale is used to represent LAI estimates corrected to early summer levels.

Table 3
FLIM-CLUS parameters

Parameter	Units	NSA-OBS	NSA-OJP	SSA-OBS	SSA-OBS	Source
θ_s	degrees	73	69	75	75	observed
H	m	7.9	10.5	9.5	9.5	Halliwell and Apps (1997)
R	m	0.45	0.90	0.50	0.50	Halliwell and Apps (1997)
Crown ellipticity	dim.	8	3	8	3	Leblanc, Bicheron, Chen, Leroy, and Cihlar (1999)
$G(\theta_s)$	dim.	0.40	0.45	0.38	0.50	Chen (1996b)
$G(\theta_v)$	dim.	0.15	0.20	0.25	0.25	Chen (1996b)
$\rho_{\text{sunlit snow}}$	ρ_{red}, ρ_{NIR}	0.79, 0.80	0.92, 0.97	0.84, 0.85	0.90, 0.96	observed
$\rho_{\text{dense canopy}}$	ρ_{red}, ρ_{NIR}	0.04, 0.20	0.05, 0.20	0.04, 0.20	0.05, 0.20	observed

θ_s is solar zenith angle.
θ_v is view zenith angle.
Crown ellipticity defined in Leblanc et al. (1999) corresponds to crown profile.
$G(\theta)$ is the ratio or plant area projected along angle θ versus to total plant area.
ρ corresponds to reflectance in CASI bands.

applied to estimate LAI and regions that are clear of overstory vegetation (open areas) where LAI is set to zero. We initially defined open area as gaps larger than that observed from in situ gap size measurements along the surface transects (2 m based on Chen, 1996a). However, mixed pixels from the 2-m imagery and shadows cast over open areas led to the use of a larger 6-m minimum size. The reflectance model should still map low (although possibly not zero) LAI over areas with gaps less than 6 m in size. K-means (Hartigan, 1975) clustering was applied to the 2-m reflectance data for each tower site to separate open areas and canopy areas. The shaded region between the canopy edge and the sunlit snow was then mapped as a tentative open area using ray tracing. A conservative approach was used where only pixels in the unknown shadowed cluster intersecting the ray-traced open areas are relabelled as open areas.

Pixels corresponding to remaining unknown areas, crown clusters, and shaded snow clusters were included in the canopy areas. A one-pixel buffer of open areas around canopy areas was relabelled as canopy areas to minimise mixed pixel effects. A modified version (Hu et al., 2000) of the Forest Light Interaction Model (FLIM) (Rosema et al., 1992) was used to map L_e in canopy areas. FLIM-CLUS parameters for the OBS stands were taken from published site measurements (Table 3). FLIM is applied to reflectance measurements corresponding to a mixture of typical shadowed and sunlit overstory and understory components in the vicinity of the region where LAI is to be estimated. Our study used a 30-m moving window average of all canopy area pixels around each 2-m grid cell at which LAI is mapped (i.e., all pixels labelled as canopy areas). In doing so, the spatial scale (footprint) of the LAI_e estimates from FLIM-CLUS varied from 2 m for open areas to up to 30 m in cases where the 30-m square around a canopy pixel is completely filled with canopy pixels. One advantage of this variable scale was that LAI_e is still estimated for isolated clumps of trees, albeit with less confidence in the assumption of stationarity of canopy properties (e.g., clumping) within the PIFOV.

The FLIM-CLUS LAI_e estimate was converted to LAI using site-specific estimates of growing season α and Ω (Chen et al., 1997). The same conversion factors were used by the surface and coarse-scale methods, so errors in these estimates cancel out during comparisons. Finally, the FLIM-CLUS LAI estimates were adjusted for seasonal differences in LAI based on the ratio of senescence and growing season surface LAI_e values for each site (Chen et al., 1997).

4.3. Coarse-scale method

Coarse-scale LAI estimates was generated using empirical relationships between spectral vegetation indices and

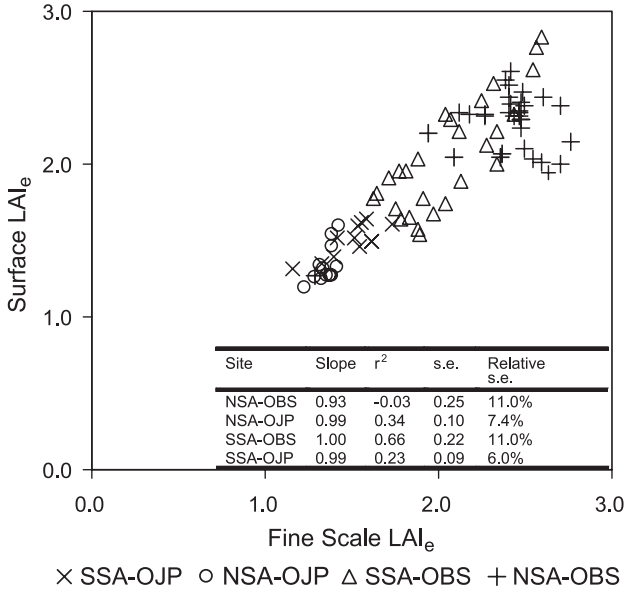

Fig. 5. FLIM-CLUS prediction of surface LAI-2000 and TRAC L_e estimates at study sites. Root mean square error of fits relative to average surface estimates are 6% at the SSA-OJP, 7% at the NSA-OJP, 10% at the SSA-OBS, and 15% at the NSA-OBS. Statistics for linear prediction of surface LAI_e using fine-scale LAI_e with intercept forced through zero are included.

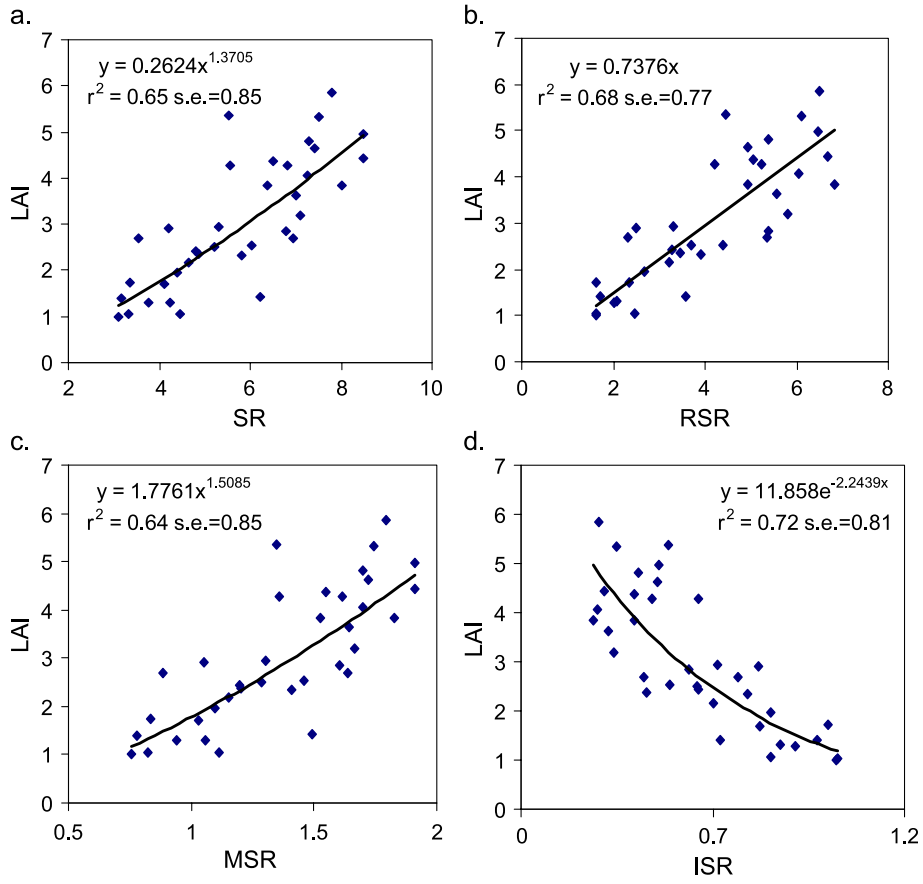

Fig. 6. Scatter plots and functional regressions between selected spectral vegetation indices and surface LAI estimates for conifer auxiliary sites within the BOREAS region. Indices are derived from summer Landsat TM reflectance estimates at 90-m scale and include (a) simple ratio (SR), (b) modified simple ratio (MSR), (c) infrared simple ratio (ISR), and (d) reduced simple ratio (RSR). Surface LAI estimates correspond to the mean LAI value (derived from a combination of LAI-2000 and TRAC measurements) over two perpendicular 50-m transects centred over each auxiliary measurement site in the BOREAS study areas.

surface estimates from the auxiliary sites. Landsat TM 5 red (0.63–0.69 μm), NIR (0.76–0.90 μm) and shortwave-infrared, SWIR (1.55–1.75 μm), 30-m PIFOV apparent reflectance images used in Brown et al. (2000) were extracted over each site. The following spectral vegetation indices were synthesized as they have demonstrated reasonable success in mapping LAI at 30-m scale:

(a) Simple ratio (SR) (Jordan, 1969)

$$\mathrm{SR} = \rho_{\mathrm{NIR}}/\rho_{\mathrm{RED}} \tag{4}$$

(b) Modified simple ratio (MSR) (Chen, 1996a,b)

$$\mathrm{MSR} = \frac{\mathrm{SR} - 1}{\mathrm{SR}^{0.5} + 1} \tag{5}$$

(c) Reduced simple ratio (RSR) (Brown et al., 2000)

$$\mathrm{RSR} = \mathrm{SR}\left(\frac{\rho_{\mathrm{SWIR,max}} - \rho_{\mathrm{SWIR}}}{\rho_{\mathrm{SWIR,max}} - \rho_{\mathrm{SWIR,min}}}\right) \tag{6}$$

(d) Infrared simple ratio (ISR) (Ahern, Erdle, Maclean, & Kneppeck, 1991)

$$\mathrm{ISR} = \rho_{\mathrm{SWIR}}/\rho_{\mathrm{NIR}} \tag{7}$$

Type II regression relationships between these indices and LAI over the 46 sites were applied assuming equal measurement uncertainty between LAI and vegetation indices. This assumption is appropriate for the simple ratio (Fernandes et al., 2001) and is likely less biased than assuming no measurement errors for the other indices. The stands include both NSA and SSA to allow for sufficient sampling across the entire range of LAI.

The Landsat TM 5 reflectance images were manually registered to the CASI data with precision given in Table 1. A rectangular moving window was used to aggregate each Landsat image to successively coarser spatial scales gridded at 30-m resolution. The regression relationships were applied to these coarse-scale images to produce coarse-scale LAI estimates.

4.4. Comparison method

Given that the scale we used to estimate LAI was always coarser than the grid resolution, all of the estimates were oversampled in space. It was possible to subsample, but this would result in very few data points for coarse-scale estimates (e.g., perhaps only 1 LAI value for a site at 1-km scale). The subsampled site mean LAI estimate would also be biased by the position of the coarse-scale PIFOV center. For example, placing the single 1-km pixel at the center of the site would misrepresent the LAI estimated if the swath of a real coarse-scale sensor is such that the nearest pixel center lies at the edge of the site. Oversampling prevented the application of statistical tests of hypotheses that rely on spatial independence. Rather, the coarse-scale LAI maps represent a best case LAI estimate for a given grid cell at that scale.

4.4.1. Comparison with surface estimates

Comparisons of surface and fine-scale estimates were performed by overlaying the surface transects on the georeferenced CASI images. One issue was the need to match the spatial footprint of surface and fine-scale estimates. The footprint for LAI-2000 estimates is a circle with a radius ranging from 24 m at the NSA-OBS to 45 m at the SSA-OJP. To match surface and fine-scale footprints, a 30-m moving average filter is applied to the fine-scale 2-m grid resolution images. The smoothed fine-scale values corresponding to the 2-m resolution pixel coincident with each center transect sample point was then compared to the nine-point average of LAI-2000 samples centred in a 10-m radius of the center sample point.

Only site mean surface and coarse-scale estimates were compared as it was not possible to register the TM imagery with sufficient accuracy to screen out surface samples at the edges of pixels rather than within a pixel.

4.4.2. Comparison of image-based estimates

Comparisons of the spatial patterns of fine- and coarse-scale LAI require consideration of registration errors between both image sources. The area of sliver polygons when comparing the same mapping unit in both LAI maps will then be a function of the extent of size of the mapping unit and the registration error. When overlaying equal size rectangular mapping units, the ratio of maximum possible sliver polygon area relative to mapping unit area (R) is given by

$$R = \begin{cases} 1 & \delta x > w \cup \delta y > l \\ \dfrac{l\delta x + w\delta y - \delta x\delta y}{lw} & \text{else} \end{cases} \quad (8)$$

Where δx and δy is the registration error along the lengths (l) and widths (w) of the mapping unit. We used a rectangular moving average filter to smooth (increase mapping unit scale or footprint) each image so the maximum overlay error was less than 15% of the area (100 m for OBS sites and 150 m for OJP sites). Smoothing was not required for 500-m and 1-km coarse-scale images, as they already met the minimum scale criteria. Coarsening the scale of the maps did not imply that all of the estimates are produced at a scale coarser than 30 m. It simply restricted the comparison between fine and coarse estimates to a coarser scale.

4.5. Comparison metrics

Surface and fine-scale estimates were compared on the basis of the root mean square error expressed as a percentage of the mean surface LAI_e (i.e., the relative root mean square error or rrmse). The slope, coefficient of determination, and standard error of the best linear fit constrained through the origin was included. However, the actual fine-scale maps were not adjusted for biases between surface and fine-scale values. Furthermore, although the coefficient of determination was included, the surface transects were likely not representative of the expected distribution of LAI_e over the sites.

Fine- and coarse-scale estimates were compared using the relative mean difference (rmd). The rmd was defined as $100 \times$ (coarse-scale site mean value − fine-scale site mean value)/fine-scale site mean value. The sample correlation coefficient, ρ, was also used to compare spatial patterns of fine-scale and coarse-scale estimates. The rmd describes the bias between fine-scale and coarse-scale estimates, while ρ speaks to the precision of the estimates. Again, the metrics

Table 4
Relative mean difference (rmd) in % and Pearson correlation coefficients between fine-scale and coarse-scale LAI estimates

Site	Index	Relative mean difference			Pearson correlation coefficient		
		Scale (m)			Scale (m)		
		30	500	1000	30	500	1000
NSA-OBS	SR	−8	−5	−4	0.59	0.40	0.17
	RSR	−3	−6	−6	**0.78**	0.56	0.34
	ISR	**2**	12	11	0.66	**0.58**	**0.43**
	MSR	−10	**−4**	**−3**	0.56	0.39	0.12
NSA-OJP	SR	13	3	5	0.50	0.46	0.34
	RSR	**0**	−10	−9	**0.64**	**0.52**	**0.35**
	ISR	4	**−3**	4	0.52	0.45	0.29
	MSR	13	−4	**−1**	0.58	0.48	0.34
SSA-OBS	SR	85	85	85	0.60	0.66	0.24
	RSR	82	77	77	**0.70**	**0.68**	**0.33**
	ISR	63	**74**	**74**	0.59	0.51	0.31
	MSR	**40**	86	86	0.60	0.65	0.20
SSA-OJP	SR	64	48	39	0.57	0.61	0.59
	RSR	51	36	28	**0.69**	0.65	0.62
	ISR	30	**29**	**23**	0.67	**0.67**	**0.64**
	MSR	**24**	43	35	0.66	0.64	0.62

Smallest absolute values of rmd and largest correlations for a given site and scale are indicated in bold.

was used as deterministic measures of agreement between LAI estimates rather than as inferential statistics.

5. Results and analyses

5.1. Surface LAI

Surface LAI estimates for the tower site transects have been previously published in Chen (1996b). Comparison of these optical estimates with spatially coincident allometric estimates result in site mean differences of 4% for SSA-OJP, 9% for NSA-OBS, 16% for NSA-OJP, and 45% for SSA-OJP (Chen et al., 1997). Since seasonal variability in LAI_e is typically less than 5% for the NSA-OBS and the stand had not been disturbed since 1994, it is likely that the additional surface estimates from 1999 are valid for comparison to 1994 data. Surface transects in the OBS sites are coincident with higher canopy cover regions (Figs. 1 and 3) and therefore may represent a bias estimate of site LAI (site mean LAI is reported in Table 2).

5.2. Surface vs. fine scale

Surface and fine-scale LAI_e estimates show relatively good agreement for all sites as indicated by the linear regression fits at each site (Fig. 5). LAI_e rather than LAI estimates are compared over individual locations within each site, as both surface and fine-scale methods use the same conversion factors for each site, and the LAI_e estimates have higher precision than LAI does. The OBS results have been previously given in Fernandes et al. (2003) and are included here for convenience. Except for the SSA-OBS, the fits are forced through zero due to the lack of low LAI measurements along the transects. Forcing the fits through zero ensures the coefficient of determination and standard error correspond to physically meaningful line fits.

At all sites, the slope of the fitted line (Fig. 5) is not significantly different from one at a 95% confidence level. The near 1:1 relationship between fine-scale and surface LAI_e estimates adds confidence to the use of fine-scale estimates in areas outside the surface transects. The rrmse

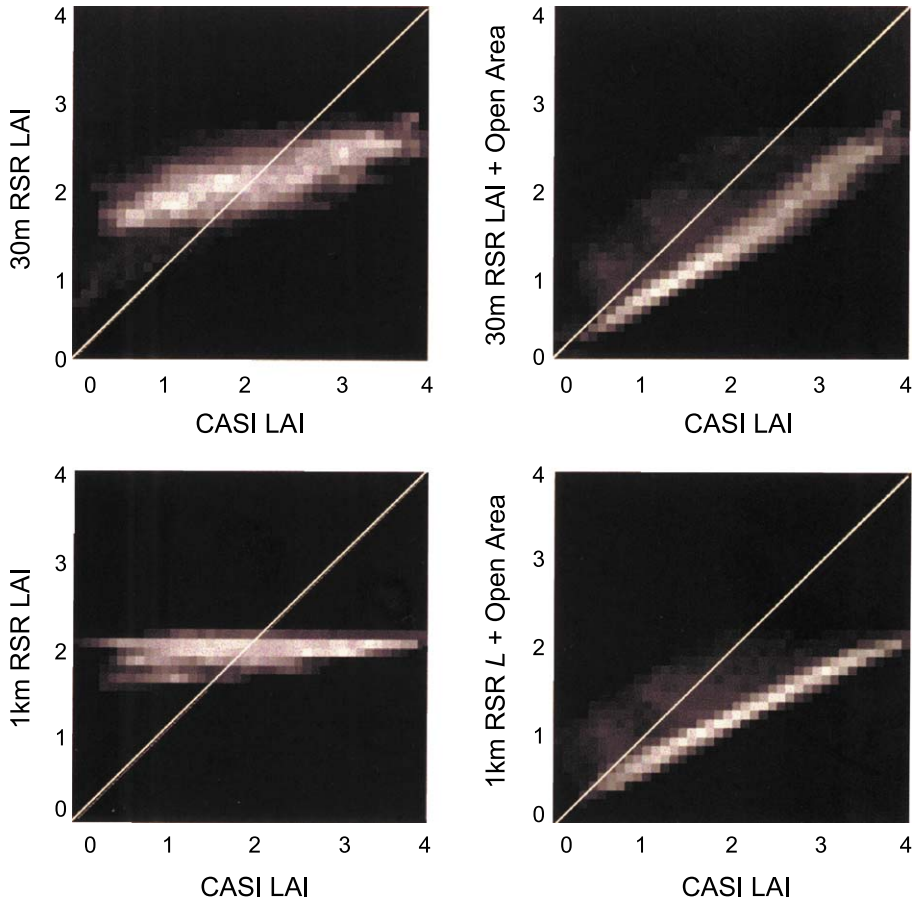

Fig. 7. Density plots comparing fine-resolution CASI LAI and coarser resolution Landsat TM-based LAI for the NSA-OBS. Landsat TM LAI estimates are derived using the reduced simple ratio at 30-m scale (upper left) and at 1-km scale (lower right). Plots on the right correspond to specification of open areas in the Landsat TM images based on processing the CASI image using FLIM-CLUS. All comparisons are performed after applying a 100-m moving window average to each LAI map and subsampling every 100 m, so that registration errors do not affect results. The 1:1 line is indicated.

of LAI_e is under 8% for the OJP sites and 14% for the SSA-OBS site. This level of precision is close to the sum of uncertainties due to LAI_e estimation and seasonal correction. The additional uncertainty in matching the spatial footprint of the LAI-2000 and CASI estimates may explain larger differences such as the overestimates at the NSA-OBS.

Evaluation of site mean differences in LAI are meaningful both because precision errors should decrease for mean values and because modellers typically require LAI rather than LAI_e. Site mean surface LAI is 80% greater than fine-scale values at both OBS sites (Table 2). The fact that the surface and fine-scale estimates are in agreement over the transects but not over an entire site suggests that residuals are concentrated in open areas that are not well represented by the transects. This explanation is further supported in that the surface LAI estimates are larger than the fine-scale values and that at the OJP sites, where open areas are not substantial, the surface LAI estimates are only 20% larger (in contrast to 80% at the OBS sites) than the fine-scale estimates. There are insufficient surface data to validate the fine-scale open areas in situ. However, *X* clusters used to define the open areas are spectrally distinct from other classes (Fernandes et al., 2002). Isolated clumps of trees are unlikely to fall in the open area class due to the contrast in the red band of vegetation and snow and the use of a one-pixel buffer when defining canopy areas that reduces the chance of missing a mixed pixel containing a partial tree crown.

5.3. Surface vs. coarse scale

Type II regressions between Landsat TM-based vegetation indices and surface LAI at auxiliary sites showed relatively similar coefficient of determination (0.64–0.72) and standard error (0.71–0.85) irrespective of index (Fig. 6). As such, we focus our discussion on LAI estimates from the reduced simple ratio (see Figs. 1–4 and Table 2), as it corresponds to the same spectral index used to produce archived images for these sites (Chen & Cihlar, 1998). The coarse-scale site mean estimates using 30-m-scale imagery are 80% lower than surface for the NSA-OBS, 18% lower for the NSA-OJP, 2% larger for the SSA-OBS, and 34% larger for the SSA-OJP. These biases remain when using 1-km-scale RSR estimates. Site mean LAI estimates at 30-m

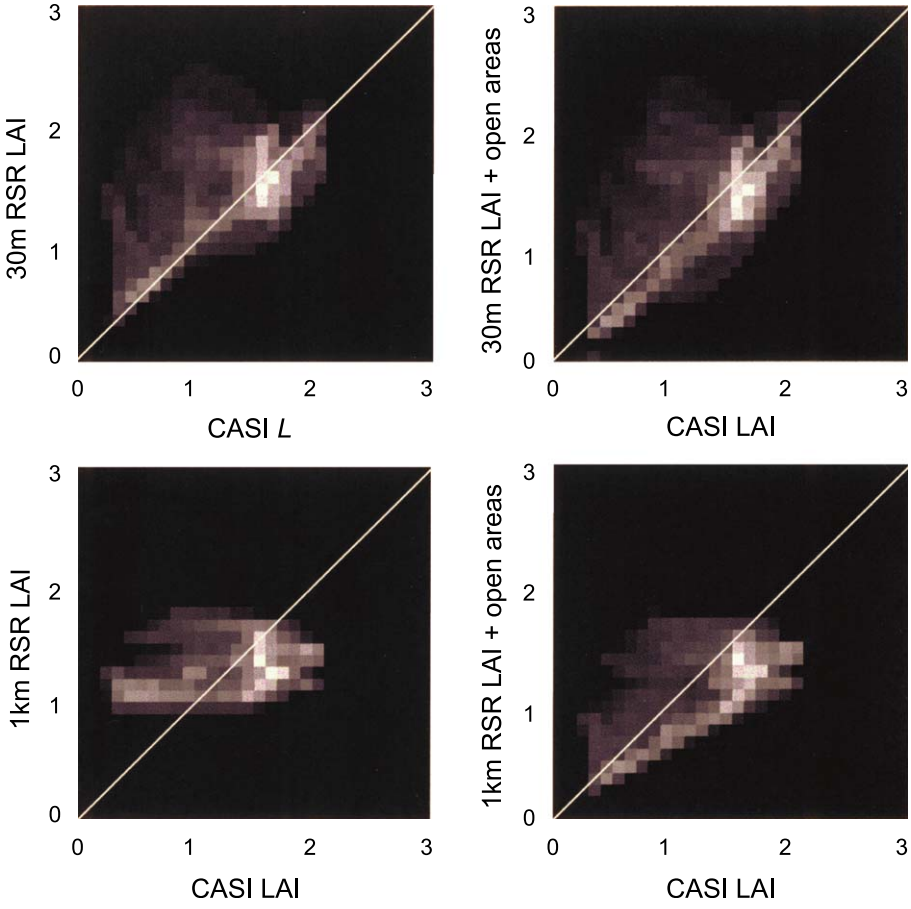

Fig. 8. Density plots comparing fine-resolution CASI LAI and coarser resolution Landsat TM-based LAI for the NSA-OJP. Landsat TM LAI estimates are derived using the reduced simple at 30-m scale (upper left) and at 1-km scale (lower right). Plots on the right correspond to specification of open areas in the Landsat TM images based on processing the CASI image using FLIM-CLUS. All comparisons are performed after applying a 100-m moving window average to each LAI map and subsampling every 100 m, so that registration errors do not affect results. The 1:1 line is indicated.

scale should have substantially lower standard deviation than the per pixel errors, indicated by the regression standard error (see Fig. 6), as there should be a large number of statistically independent pixels. Therefore, the differences between surface and coarse-scale estimates are likely due to either systematic errors in reflectance estimates or nonrandom residuals in the spectral index versus LAI regressions. Pooling of NSA and SSA data may have resulted in some bias in residuals. However, using an RSR versus LAI regression developed using only NSA auxiliary sites only increased NSA-OBS LAI by 4%. Atmospheric correction errors are unlikely to explain the differences between surface and coarse scale since coarse-scale LAI was derived from the same images over which calibration is performed.

5.4. Fine scale vs. coarse scale

Site mean coarse-scale estimates of LAI are similar in values to fine-scale estimates at the NSA-OBS and NSA-OJP but consistently higher in the SSA-OBS (between 40% and 85%) and SSA-OJP (between 24% and 64%). The similarity in rmd between 500 m and 1 km comparisons suggests that much of the scaling error is already encountered with 500-m-resolution imagery. Similarity in rmd across the indices used, combined with the high accuracy of the fine-scale estimates (as indicated by good agreement with surface values along transects) suggests that the coarse-scale LAI maps are biased and that the lower fine-scale site mean LAI may be due to the accurate delineation of open areas at fine scale with FLIM-CLUS.

Agreement between fine- and coarse-scale LAI patterns varies substantially, with ρ typically between 0.50 and 0.95 (Table 4). RSR consistently produces the highest ρ values at 30-m scale. This may be related to the RSR's ability to reduce the impact of understory variability on overstory LAI estimates (Brown et al., 2000). The ρ decreases by an average of 35% between 500-m and 1-km scale. This suggests that extreme LAI values are lost between 500 m and 1 km irrespective of index or site. Density plots (Figs. 7–10) comparing fine-scale LAI vs. coarse-scale RSR LAI at 30-m and 1-km scale support this hypothesis.

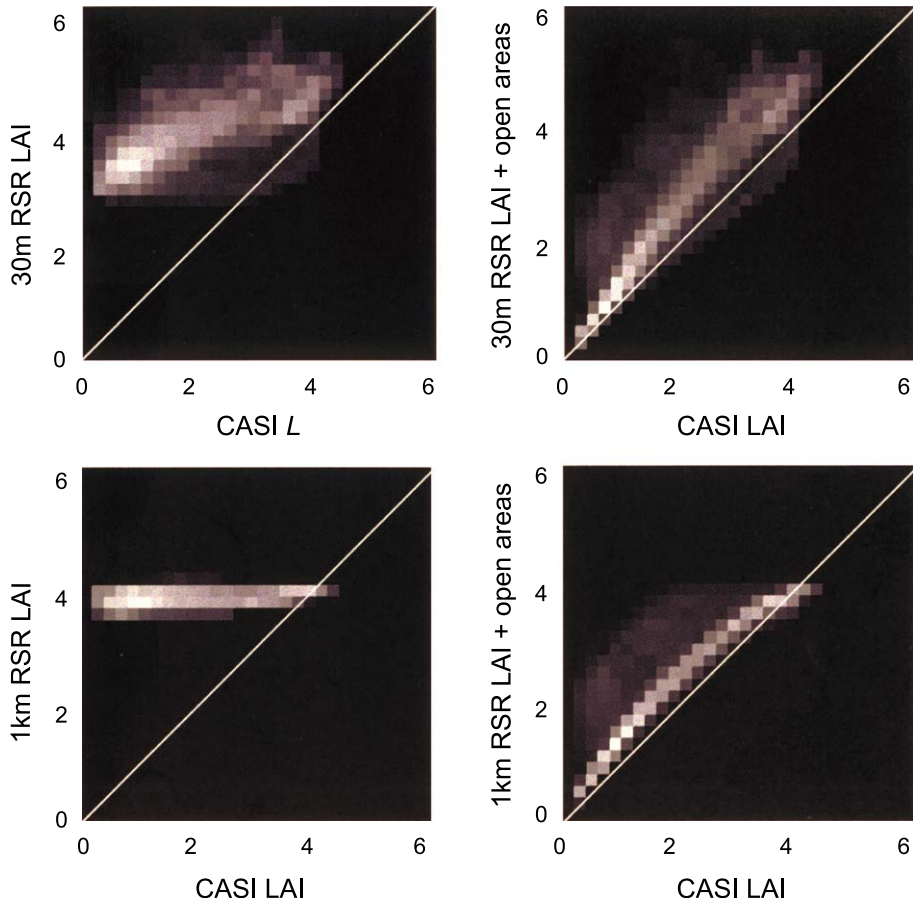

Fig. 9. Density plots comparing fine-resolution CASI LAI and coarser resolution Landsat TM-based LAI for the SSA-OBS. Landsat TM LAI estimates are derived using the reduced simple ratio at 30-m scale (upper left) and at 1-km scale (lower right). Plots on the right correspond to specification of open areas in the Landsat TM images based on processing the CASI image using FLIM-CLUS. All comparisons are performed after applying a 100-m moving window average to each LAI map and subsampling every 100 m, so that registration errors do not affect results. The 1:1 line is indicated.

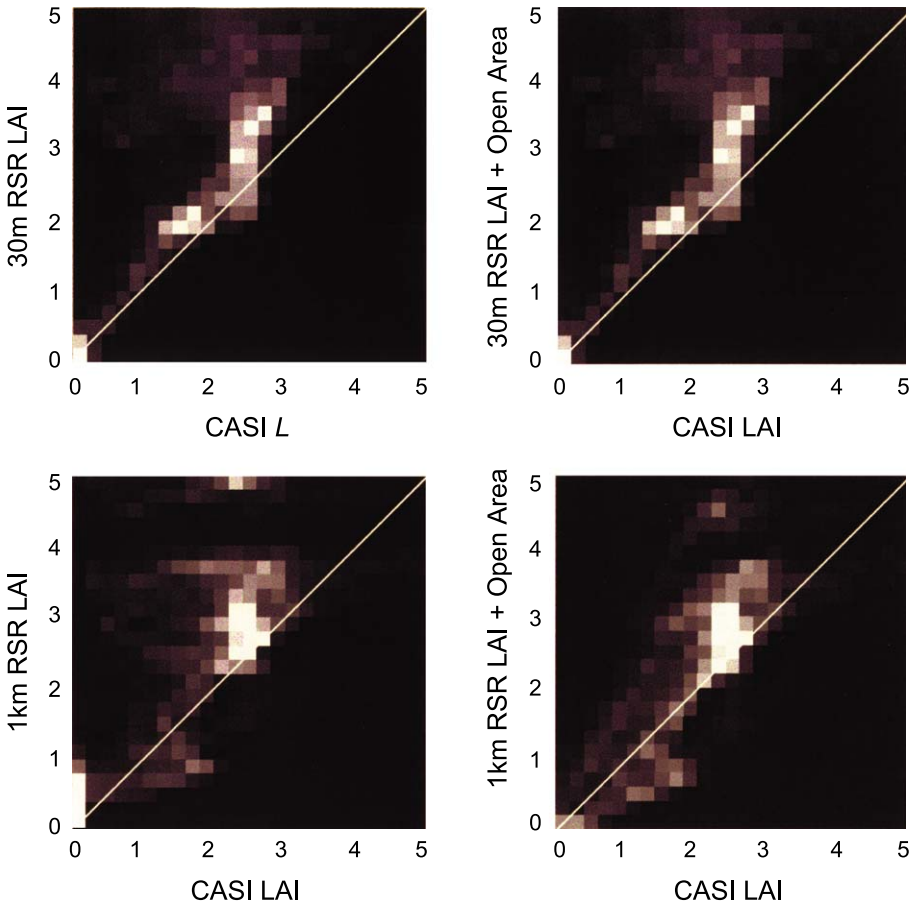

Fig. 10. Density plots comparing fine-resolution CASI LAI and coarser resolution Landsat TM-based LAI for the SSA-OJP. Landsat TM LAI estimates are derived using the reduced simple ratio at 30-m scale (upper left) and at 1-km scale (lower right). Plots on the right correspond to specification of open areas in the Landsat TM images based on processing the CASI image using FLIM-CLUS. All comparisons are performed after applying a 100-m moving window average to each LAI map and subsampling every 100 m, so that registration errors do not affect results. The 1:1 line is indicated.

5.5. Role of open areas in scaling errors

Scaling errors as represented by magnitude of the rmd values are lower for the NSA than SSA sites. FLIM-CLUS predicts less open area in the NSA sites than at SSA sites. We considered the hypothesis that differences in scaling errors between sites may be chiefly due to errors over open areas in coarse-scale maps by imposing the 2-m-resolution fine-scale open area regions into the coarse-scale maps. The increased agreement (as indicated by comparing correlation coefficients between Tables 4 and 5 and the density plots in Figs. 7–10) between fine- and coarse-scale patterns after specifying open areas is expected given that the same fine-scale open areas are used in both images. However, the relative improvement is indicative of the importance of open areas in comparison to LAI patterns within canopy areas in contributing to scaling errors. Once again, scaling errors in the vegetation indices likely causes the observed scaling error in LAI since the LAI algorithms are almost linear functions of vegetation index. This phenomenon has been demonstrated for LAI scaling errors due to sub-pixel water bodies (Chen, 1999). The fine-scale vegetation index will exhibit the largest difference between open and canopy areas, and therefore, scaling errors will be largest at the edges of open areas. The OBS sites exhibit a median relative increase in ρ of 49%, while the OJP sites exhibit a median relative increase of 23%. The larger improvement at the OBS sites is possibly due to the larger proportion of open areas within these sites.

While specifying open areas increases spatial agreement, it only reduced rmd over the SSA sites. The fact that the rmd magnitude increases at the NSA-OBS site even though ρ increases substantially (compare Tables 4 and 5 for NSA sites) points to a bias error in either the fine- or coarse-scale LAI estimates in NSA-OBS closed canopy areas. Given that the fine-scale estimates matches the surface LAI values in the NSA-OBS relatively well, the error may be attributed to a substantial underestimate in closed canopy LAI with the coarse-scale maps. This, in turn, suggests that regression residuals in the empirical relationships applied to generate coarse-scale estimates may produce spatially autocorrelated residuals. With the exception of the NSA-OBS, all of the open area corrected coarse-scale site mean LAI estimates fall within the

Table 5
Relative mean difference (rmd) in % and Pearson correlation coefficients between fine-scale and coarse-scale LAI estimates that include specification of fine-scale open areas

Site	Index	L2 vs. L3			L2 vs. L3+ open area		
		Scale (m)			Scale (m)		
		30	500	1000	30	500	1000
NSA-OBS	SR	−39	−37	−40	0.59	0.40	0.17
	RSR	−40	−37	−35	**0.78**	0.56	0.34
	ISR	**−28**	**−25**	**−33**	0.66	**0.58**	**0.43**
	MSR	−38	−36	−42	0.56	0.39	0.12
NSA-OJP	SR	**0**	**−10**	**−10**	0.50	0.46	0.34
	RSR	−10	−22	−23	**0.64**	**0.52**	**0.35**
	ISR	−10	−16	−27	0.52	0.45	0.29
	MSR	−1	−15	−15	0.58	0.48	0.34
SSA-OBS	SR	19	16	15	0.60	0.66	0.24
	RSR	18	12	10	**0.70**	**0.68**	**0.33**
	ISR	**5**	**9**	**8**	0.59	0.51	0.31
	MSR	−11	16	15	0.60	0.65	0.20
SSA-OJP	SR	36	23	15	0.57	0.61	0.59
	RSR	31	17	8	**0.69**	0.65	0.62
	ISR	**9**	**11**	**5**	0.67	**0.67**	**0.64**
	MSR	34	22	15	0.66	0.64	0.62

Smallest absolute values of rmd and largest correlations for a given site and scale are indicated in bold.

uncertainty of the combined fine- and coarse-scale standard error (about 1 LAI unit).

6. Conclusions and future research

There is good agreement between spatially coincident estimates of surface and airborne LAI_e over all sites. The fact that the relationship between FLIM-CLUS and surface LAI_e is nearly 1:1 for all sites lends confidence in the simplifying assumptions embedded in FLIM-CLUS. It should be remembered that the sites have relatively uniform stand structure and species composition (excepting the large gaps in the OBS sites). The effectiveness of FLIM-CLUS may be reduced over mixed forests or larger sites. Site mean LAI differed substantially between surface and airborne techniques. The 80% overestimate at the OBS sites has implications on the interpretation of the results of modelling studies that have used these sites for validation with the surface LAI as input. We hypothesise that these differences are due chiefly to spatial autocorrelation in residuals of the calibration equations used to predict LAI from coarse-scale reflectance.

Spatial patterns of airborne and 30-m spectral index-based LAI match reasonably well at 30-m scale. The correspondence between spatial patterns is poor at 1-km scale. Specification of open areas substantially improves the agreement in spatial patterns at the OBS sites. This confirms the qualitative impression that open regions large enough to be mapped as zero LAI, but small enough to be missed by coarser scale sensors, may impact on LAI estimates in sparse boreal conifer stands.

The poor correspondence between 1-km and airborne LAI spatial patterns may not have been as distinct if we had adopted 30-m TM-based *L* maps as our fine-scale standard. Differences between 30-m TM LAI and surface site mean LAI, in spite of good correspondence with fine-scale patterns, suggests residuals in TM LAI estimates are spatially correlated. The extent of this correlation needs investigation but requires fine-scale LAI estimates for validation. Based on the results from this study, we suggest that the assumption that variability in TM LAI errors will average out over say 1 km is not always valid. As such, comparison of TM LAI estimates with other LAI maps and the use of TM LAI estimates in models may produce residuals in results that are also spatially correlated.

A number of moderate and coarse resolution current and future sensors (Advanced Very High-Resolution Radiometer, Moderate-Resolution Imaging Spectrometer, Multiple Angle Imaging Spectro Radiometer, SPOT-Vegetation, Medium-Resolution Imaging Spectrometer Instrument, and Global Land Imager) offer the potential for large area LAI mapping at frequent time intervals. The PIFOV of these sensors is larger than their gridded resolution (typically, the PIFOV at nadir is engineered to be at least twice the sampling resolution to meet the Nyquist criterion). In addition, resampling, atmosphere blurring, compositing, and off-angle viewing increase the effective spatial scale. As such, there may be instances where the sensors do not offer sufficient detail to map LAI patterns or to estimate LAI without bias. Our study offers one methodology for evaluating these LAI maps at a spatial scale that is likely near the limit of orbital passive optical systems. We identify four avenues for further research:

1. Using reflectance models to identify the uncertainty in LAI retrievals due to mixtures of open and closed canopy areas;
2. Using a sampling of high-resolution images, airborne LIDAR or intensive surface sampling to characterise stand-scale clumping;
3. Using multiangle information to explicitly map sub-pixel clumping;
4. Using hyperspectral indices that are not as sensitive to canopy geometry as broadband nadir vegetation indices.

Acknowledgements

Funding was provided by NCE-GEOIDE and a BOREAS Follow-on Grant from NSERC. Data and comments from M. Beauchemin, L. Brown, S. Leblanc, and H.P. White are appreciated.

References

Ahern, F. J., Erdle, T., Maclean, D. A., & Kneppeck, I. D. (1991). A quantitative relationship between forest growth rates and Thematic

Mapper reflectance measurements. *International Journal of Remote Sensing*, *12*(3), 387–400.

Bicheron, P., & Leroy, M. (1999). A method of biophysical parameter retrieval at global scale by inversion of a vegetation reflectance model. *Remote Sensing of Environment*, *67*, 251–266.

Bonan, G. B. (1993). Importance of leaf area index and forest type when estimating photosynthesis in boreal forests. *Remote Sensing of Environment*, *43*, 303–313.

Brown, L., Chen, J. M., Leblanc, S. G., & Cihlar, J. (2000). A shortwave infrared modification to the simple ratio for LAI retrieval in boreal forests: An image and model analysis. *Remote Sensing of Environment*, *71, 16–25.*

Chen, J. M. (1996a). Canopy architecture and remote sensing of FPAR absorbed by boreal conifer forests. *IEEE Transactions on Geoscience and Remote Sensing*, *34*(6), 1353–1368.

Chen, J. M. (1996b). Evaluation of vegetation indices and a modified simple ratio for boreal applications. *Canadian Journal of Remote Sensing*, *22*(3), 229–242.

Chen, J. M. (1999). Spatial scaling of a remotely sensed surface parameter by contexture. *Remote Sensing of Environment*, *69*, 30–42.

Chen, J. M., & Black, T. A. (1992). Defining leaf area index for non-flat leaves. *Plant, Cell and Environment*, *15*, 421–429.

Chen, J. M., & Cihlar, J. (1996). Retrieving leaf area index of boreal conifer forests using Landsat TM images. *Remote Sensing of Environment*, *55*(2), 153–162.

Chen, J. M., & Cihlar, J. (1998). *BOREAS RSS-07 LAI, Gap Fraction, and fPAR Data*. Available online at http://www-eosdis.ornl.gov/ from the ORNL Distributed Active Archive Center, Oak Ridge National Laboratory, Oak Ridge, TN, USA.

Chen, J. M., & Cihlar, J. (1999). *BOREAS RSS-07 Regional LAI and FPAR Images From Ten-Day AVHRR-LAC*. Available online at http://www-eosdis.ornl.gov/ from the ORNL Distributed Active Archive Center, Oak Ridge National Laboratory, Oak Ridge, TN, USA.

Chen, J. M., Leblanc, S. G., Miller, J. R., Freemantle, J., Loechel, S. E., Walthall, C. L., Innanen, K. A., & White, H. P. (1999). Compact Airborne Spectrographic Imager (CASI) used for mapping biophysical parameters of boreal forests. *Journal of Geophysical Research, BOREAS Special Issue II*, *104*(D22), 27945–27958.

Chen, J. M., Rich, P. M., Gower, S. T., Norman, J. M., & Plummer, S. (1997). Leaf area index of boreal forests: Theory, techniques and measurements. *Journal of Geophysical Research, BOREAS Special Issue*, *102*(D24), 29429–29443.

Cohen, W. B., & Justice, C. O. (1999). Validating MODIS terrestrial ecology products: Linking in situ and satellite measurements. *Remote Sensing of Environment*, *70*, 1–4.

Dang, Q. -L., Margolis, H. A., Sy, M., Coyea, M. R., Collatz, G. J., & Walthall, C. L. (1997). Profiles of PAR, nitrogen and photosynthetic capacity in the boreal forest: Implications for scaling from leaf to canopy. *Journal of Geophysical Research, BOREAS Special Issue*, *102*(D24), 28845–28860.

Fernandes, R. A., Hu, B., Miller, J. R., & Rubinstein, I. (2002). A multiscale approach to mapping effective leaf area index in boreal *Picea mariana* stands using high spatial resolution CASI imagery. *International Journal of Remote Sensing*, *23*(18), 3547–3568.

Fernandes, R. A., White, H. P., Leblanc, S. G., Pavlic, G., McNairn, H., Chen, J. M., & Hall, R. J. (2001). Examination of error propagation in relationships between leaf area index and spectral vegetation indices from Landsat TM and ETM. *Proceedings of the 23rd Canadian Remote Sensing Symposium, Quebec City, Quebec, August 2001* (pp. 41–51). Foy, Quebec: Universite de Laval Ste.

Frolking, S., Goulden, M. L., Woofsy, S. C., Fan, S. -M., Sutton, D. J., Munger, J. W., Bazzaz, A. M., Daube, B. C., Crill, P. M., Aber, J. D., Band, L. E., Wang, X., Savage, K., Moore, T., & Harriss, R. C. (1996). Temporal variability in the carbon balance of a spruce/moss boreal forest. *Global Change Biology*, *2*, 343–366.

Gower, S. T., Vogel, J., Stow, T., Norman, J., Steele, S., & Kucharik, C. (1997). Carbon distribution and above ground net primary production in aspen, jack pine and black spruce stands in Saskatchewan and Manitoba, Canada. *Journal of Geophysical Research, BOREAS Special Issue*, *102*(D24), 29029–29042.

Gray, L., Freemantle, J., Shepherd, P., Miller, J. R., Harron, J., & Hersom, C. (1997). Characterisation and calibration of CASI airborne image spectrometer for BOREAS. *Canadian Journal of Remote Sensing*, *23*, 188–195.

Halliwell, D. H., & Apps, M. J. (1997). BOReal Ecosystem-Atmosphere Study (BOREAS) biometry and auxillary sites: Overstory and understory data. *Natural Resources Canada, Canadian Forest Service*. Edmonton, Alberta: North. For. Cent., 254 pp.

Hartigan, J. A. (1975). *Clustering algorithms*. New York: Wiley.

Horler, D. N. H., & Ahern, F. J. (1986). Forestry information content of Thematic Mapper data. *International Journal of Remote Sensing*, *7*(3), 405–428.

Hu, B., Iannen, K., & Miller, J. R. (2000). Retrieval of leaf area index and canopy closure from CASI data over the BOREAS flux tower site. *Remote Sensing of Environment*, *74*, 255–274.

Jordan, C. F. (1969). Derivation of leaf-area index from quality of light on the forest floor. *Ecology*, *50*(2), 663–666.

Justice, C., Starr, D., Wickland, D., Privette, J., & Suttles, T. (1998). EOS land validation coordination: An update. *Earth Observer*, *10*(3), 55–60.

Kendall, M., & Stuart, A. (1951). *The advanced theory of statistics*, *vol. 2*. New York: Hafner.

Kimball, J. S., Running, S. W., & Saatchi, S. S. (1999). Sensitivity of boreal forest regional water flux and net primary productivity simulations to sub-grid-scale land cover complexity. *Journal of Geophysical Research*, *104*(D22), 27789–27801.

Kimball, J. S., Thornton, P. E., White, M. A., & Running, S. W. (1997). Simulating forest productivity and surface-atmosphere carbon exchange in the BOREAS study region. *Tree Physiology*, *17*, 589–599.

Kimball, J. S., White, M. A., & Running, S. W. (1997). BIOME-BGC simulations of stand hydrologic processes for BOREAS. *Journal of Geophysical Research, BOREAS Special Issue*, *102*(D24), 29043–29052.

Knyazikhin, Y., Glassy, J., Privette, J. L., Tian, Y., Lotsch,, A., Zhang, Y., Wang, Y., Morisette, J. L., Votava, P., Myneni, R. B., Nemani, R. R., & Running, S. W. (2000). *MODIS/Terra Leaf Area Index/FPAR 8-day L4 Global 1 km ISIN Grid*. Available via http://edcdaac.usgs.gov from EROS Data Center, USA.

Leblanc, S. G., Bicheron, P., Chen, J. M., Leroy, M., & Cihlar, J. (1999). Investigation of directional reflectance in boreal forests using an improved 4-scale model and airborne POLDER Data. *IEEE Transactions on Geoscience and Remote Sensing*, *37*(3), 1396–1414.

Leblanc, S. G., & Chen, J. M. (2001). A practical scheme for correcting multiple scattering effects on optical LAI measurements. *Agricultural and Forest Meteorology, 110*(2), 125–139.

Lefsky, M. A., Cohen, W. B., Acker, S. A., Parker, G. G., Spies, T. A., & Harding, D. (1999). Lidar remote sensing of the canopy structure and biophysical properties of Douglas-fir western hemlock forests. *Remote Sensing of Environment*, *70*, 339–361.

Liu, J., Chen, J. M., Cihlar, J., & Chen, W. (1999). Net primary productivity distribution in the BOREAS region from a process model using satellite and surface data. *Journal of Geophysical Research, BOREAS Special Issue II*, *104*(D22), 27735–27754.

Lucas, N. S., Curran, P. J., Plummer, S. E., & Danson, F. M. (2000). Estimating the stem carbon production of a coniferous forest using an ecosystem simulation model driven by the remotely sensed red edge. *International Journal of Remote Sensing*, *21*(4), 619–631.

Miller, J. B. (1967). A formula for average foliage density. *Australian Journal of Botany*, *15*, 141–144.

Morisette, J. T., Privette, J. L., Justice, C. O., & Running, S. W. (1999). *MODIS Land Validation Plan*. Available via http://pratmos.gsfc.nasa.gov/~justice/modland/valid.

Myneni, R. B., Nemani, R. R., & Running, S. W. (1997). Estimation of global leaf area index and absorbed par using radiative transfer models. *IEEE Transactions on Geoscience and Remote Sensing*, *35*, 1380–1393.

Nemani, R., Pierce, L., Running, S., & Band, L. (1993). Forest ecosystem processes at the watershed scale: Sensitivity to remotely-sensed leaf area index estimates. *International Journal of Remote Sensing*, *14*, 2519–2534.

Nijssen, B., Haddeland, I., & Lettenmaier, D. (1997). Point evaluation of a surface hydrology model for BOREAS. *Journal of Geophysical Research*, 102, 29, 367–29, 378.

Nilson, T. (1971). A theoretical analysis of the frequency of gaps in plant stands. *Agricultural and Forest Meteorology*, *8*, 25–38.

Nilson, T. (1999). Inversion of gap frequency data in forests stands. *Agricultural and Forest Meteorology*, *98–99*, 437–448.

Nilson, T., Anniste, J., Lang, M., & Praks, J. (1999). Determination of needle area indices of coniferous forest canopies in the NOPEX region by ground-based optical measurements and satellite images. *Agricutural and Forest Meteorology*, *98–99*, 449–462.

O'Neill, N. T., Zagolski, F., Bergeron, M., Royer, A., Miller, J., & Freemantle, J. (1997). Atmospheric correction of CASI images acquired over the BOREAS southern study area. *Canadian Journal of Remote Sensing*, *23*, 143–162.

Peddle, D. R., Hall, F. G., & LeDrew, E. F. (1999). Spectral mixture analysis and geometrical–optical reflectance modeling of Boreal forest biophysical structure. *Remote Sensing of Environment*, *67*, 288–297.

Peterson, D. L., Spanner, M. A., Running, S. W., & Teuber, K. B. (1987). Relationship of Thematic Mapper Simulator data to leaf area index of temperate conifer forests. *Remote Sensing of Environment*, *22*, 323–341.

Rosema, A. W., Verhoef, W., Noorbergen, H., & Borgesius, J. J. (1992). A new forest light interaction model in support of forest monitoring. *Remote Sensing of Environment*, *42*, 23–41.

Running, S. W., Peterson, D. L., Spanner, M. A., & Teuber, K. B. (1986). Remote sensing of forest leaf area index. *Ecology*, *67*, 273–275.

Schaudt, K. J., & Dickinson, R. E. (2000). An approach to deriving roughness length and zero-plane displacement height from satellite data, prototyped with BOREAS data. *Agricultural and Forest Meteorology*, *104*, 143–155.

Sellers, P. J., Hall, F. G., Apps, M., Baldocchi, D., Cihlar, J., den Hartog, J., Goodison, B., Kelly, R. D., Lettenmeir, D., Margolis, H., Nelson, A., Ranson, J., Roulet, N., & Ryan M., (1993). *BOREAS experiment plan (Version 1.0)*. NASA/GSFC, Greenbelt, Md 10771, 358 pp. plus appendices.

Spanner, M., Johnson, L., Miller, J., McCreight, R., Freemantle, J., Runyon, J., & Gong, R. (1994). Remote sensing of seasonal leaf area index across the Oregon Transect. *Ecological Applications*, *4*(2), 258–271.

Turner, D. P., Cohen, W. B., Kennedy, R. E., Fassnacht, K. S., & Briggs, J. M. (1999). Relationship between leaf area index and Landsat TM spectral vegetation indices across three temperate zone sites. *Remote Sensing of Environment*, *70*, 52–68.

Welles, J. M., & Norman, J. M. (1991). Instrument for indirect measurement of canopy architecture. *Agronomy Journal*, *83*, 818–825.

Wiscombe, W. J., & Warren, S. G. (1980). A model of the spectral albedo of snow: I. Pure snow. *Journal of the Atmospheric Sciences*, *37*(12), 2712–2733.

Wulder, M. A. (1998). The prediction of leaf area index from forest polygon decomposed through the interpretation of remote sensing, GIS, UNIX and C. *Computers and Geoscience*, *24*(2), 151–157.